Template-free Synthesis and Encapsulation Technique for Layer-by-Layer Polymer Nanocarrier Fabrication

Aisha Qi, Peggy Chan, Jenny Ho, Anushi Rajapaksa, James Friend, and Leslie Yeo*

Micro/Nanophysics Research Laboratory, RMIT University, Melbourne, VIC 3001, Australia

ABSTRACT

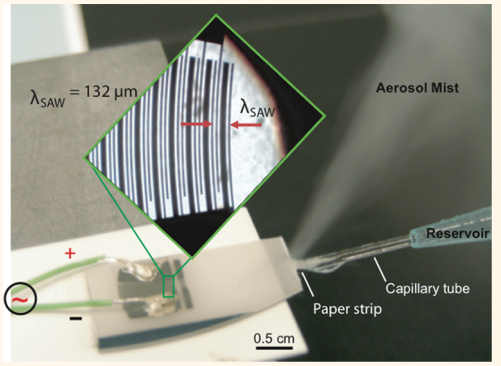

The encapsulation of therapeutic molecules within multiple layers of biocompatible and biodegradable polymeric excipients allows exquisite design of their release profile, to the extent the drug can be selectively delivered to a specific target location *in vivo*. Here, we develop a novel technique for the assembly of multilayer polyelectrolyte nanocarriers based on surface acoustic wave atomization as a rapid and efficient alternative to conventional layer-by-layer assembly, which requires the use of a sacrificial colloidal template over which consecutive polyelectrolyte layers are deposited. Polymer nanocarriers are synthesized by atomizing a polymer solution and suspending them within a complementary polymer solution of opposite charge subsequent to their solidification in-flight as the solvent evaporates; reatomizing this suspension produces nanocarriers with a layer of the second polymer deposited over the initial polymer core. Successive atomization—suspension layering steps can then be repeated to produce as many additional layers as desired. Specifically, we synthesize nanocarriers comprising two and three, and up to eight, alternating layers of chitosan (or polyethyleneimine) and carboxymethyl cellulose within which plasmid DNA is encapsulated and show *in vitro* DNA release profiles over several days. Evidence that the plasmid's viability is preserved and hence the potential of the technique for gene delivery is illustrated through efficient *in vitro* transfection of the encapsulated plasmid in human mesenchymal progenitor and COS-7 cells.

KEYWORDS:

Nanocarriers comprising multiple polyelectrolyte assemblies whose properties (*e.g.*, dimension, composition, stability, and functionality) can be specifically tuned allow precise control over not only the biocompatibility of each layer to a specific targeted *in vivo* region but also the selective release of the drug within each region.[1] This is extremely attractive for a broad range of applications across drug delivery, regenerative medicine, medical imaging, biomolecular sensing, catalysis, and even cosmetics,[2] in addition to their utility as microscale reactors for chemical synthesis within confined environments.[3] To date, the prevalent method for synthesizing multilayer carriers is the so-called layer-by-layer (LbL) approach. First demonstrated for the assembly of multiple polymer layers on rigid planar substrates,[4] the LbL technique has been extended to engineer hollow multilayered carriers by the stepwise alternate deposition of oppositely charged polyelectrolytes onto a colloidal particle template, which is then sacrificially removed.[5] Drug loading into these multilayered carriers however poses some challenges. Molecular diffusion through pH-controlled pores in the carrier,[6] while simple, is plagued by low loading efficiency and poor reproducibility,[7] and is limited to drug molecules that are sufficiently small to permeate through.[2] Enhancing the loading efficiency through the use of smaller molecular agents with high affinity for the drug is limited to the possibility of finding an appropriate sequestration agent that does not invoke an undesirable inflammatory response.[2,8] While it is possible to directly deposit the polymer layers onto a drug crystal template[9] or a porous colloidal template containing the drug,[10] this relies on the formation of drug crystals or additional steps to sacrifically remove the porous core. Moreover, LbL methods are laboratory-based batch processes with limited scalability.

Reminiscent of a related technique employed for polyelectrolyte carrier patterning,[11] microfluidics has enabled a route for large-scale, continuous production of multilayer carriers with a diversity of customizable physicochemical properties.[12,13] Liquid

* Address correspondence to leslie.yeo@rmit.edu.au.

Received for review July 26, 2011 and accepted November 7, 2011.

Published online November 07, 2011
10.1021/nn202833n

crystal droplets are made to flow within an immiscible continuous medium containing a dissolved polymer and surfactant. After polymer/surfactant coadsorption at the droplet interface, the continuous phase is replaced by a rinse solution followed by a polymer solution to form a layer; repeating the process then leads to an additional polymer layer.[12] The encapsulation of starch granules in alginate and chitosan bilayer carriers has also been demonstrated using hydrodynamic flow focusing in a microchannel. While alginate carriers are gelated using cross-linking agents and transferred from an oil continuum into a coflowing aqueous continuum by tailoring the wettability of a microchannel section, deposition of the subsequent chitosan layer however necessitated an external batch centrifugation process.[13] Moreover, not only are the channel's surface properties crucial in maintaining the desired flow, fabrication inaccuracies and the presence of contaminants also contribute to nonuniformity in carrier morphology. The most severe limitation of microfluidic LbL synthesis, however, is the lower bound on the carrier size (10−100 μm) imposed by the microchannel dimension—too large for most targeted drug delivery applications where carrier dimensions typically on the order of 100 nm are necessary.[14,15] In targeted cancer therapy, for example, the upper limit on drug particle size to extravasate tumor microvasculature is 400−600 nm, extravasation being most effective when the particles are below 200 nm.[16,17]

We report here a fast and simple aerosolization-based technique for multilayer *nano*carrier synthesis and encapsulation that retains the advantages of conventional LbL assembly but negates the necessity for a colloidal template or affinity enhancers while circumventing limitations associated with microfluidic platforms. As with the conventional LbL method, the stepwise formation of these carriers allows the possibility for the introduction of multiple functionalities such that a variety of other species such as drugs, their adjuvants, proteins and DNA could potentially be encapsulated. Moreover, the 100 nm order dimensions of the synthesized carriers are ideal for drug delivery applications. The underlying approach employed is surface acoustic wave (SAW) atomization (Figure 1a),[18] a powerful method for the generation of monodisperse, micrometer-scale aerosol droplets[19]—a platform that has already been exploited, for example, for protein extraction and characterization for paper-based diagnostics,[20] mass spectrometry interfacing with microfluidic devices,[21,22] and, most relevantly, portable pulmonary delivery of asthmatic steroids.[23]

The basis of the present technique is the possibility of using the SAW to atomize solutions of polymeric excipients or proteins such that the subsequent evaporation of the solvent in-flight after the aerosol droplets are generated leaves behind 10−100 nm dimension polymer or protein nanoparticles.[24,25] Homogeneous protein encapsulation is also possible by dispersing the protein within the polymer solution to be atomized.[26] The tedious and cumbersome procedures associated with traditional benchtop protocols for encapsulation involving polymer solvent extraction from a double emulsion by evaporation, phase separation (coacervation or precipitation) and spray drying can therefore be avoided. Moreover, lysis of shear-sensitive drug molecules is avoided, in contrast to contemporary atomization techniques using electric fields (electrospraying), bulk piezoelectric elements or Langevin transducers. This is because the time scale associated with the high frequency (>10 MHz) of the SAW is much shorter[27] than the characteristic time scale for cavitation nucleation[19] and molecular relaxation.[28] This simple SAW nanoparticle synthesis and encapsulation technique can therefore be extended to synthesize multilayer polyelectrolyte carriers by successively atomizing a polyelectrolyte solution into its oppositely charged complementary pair. To illustrate the flexibility of this technique and its practical therapeutic applicability, plasmid DNA (pDNA) is encapsulated within the nanocarriers with little added complexity and subsequently used to demonstrate good *in vitro* transfection. Altogether, the system constitutes a scalable, miniature, and inexpensive platform for precise and rapid multilayer nanocarrier synthesis.

RESULT AND DISCUSSION

The strategy for the synthesis of the multilayer polyelectrolyte nanocarriers and the encapsulation of therapeutic molecules within them is described in detail in the Methods section. Briefly, the SAW, generated when an oscillating electrical signal is applied to the electrodes shown in Figure 1b, initially atomizes the fluid containing a polymer solution delivered to the substrate (Figure 1c). As the atomized droplets travel through the heated spiral tube assembly, the solvent evaporates leaving behind solidified polymer nanocarriers which are then collected in a solution comprising a complementary polymer of opposite charge. Reatomizing this dispersion then leads to the deposition of the second complementary polymer layer over the initial polymer core. Additional polymer layers of alternating charge can subsequently be deposited by repeating the atomization−evaporation−resuspension process without requiring washing steps between coatings. This is shown with model polymers chitosan (Chi), carboxymethyl cellulose (CMC), and linear polyethyleneimine (PEI); we note that the polymer layering is relatively insensitive to processing conditions. At an atomization rate of 0.2 mL/min, the number density of nanocarriers synthesized, allowing for losses, is around $10^3/\mu$L. Evidence of the consecutive layering of these polymers is provided through zeta-potential measurements and

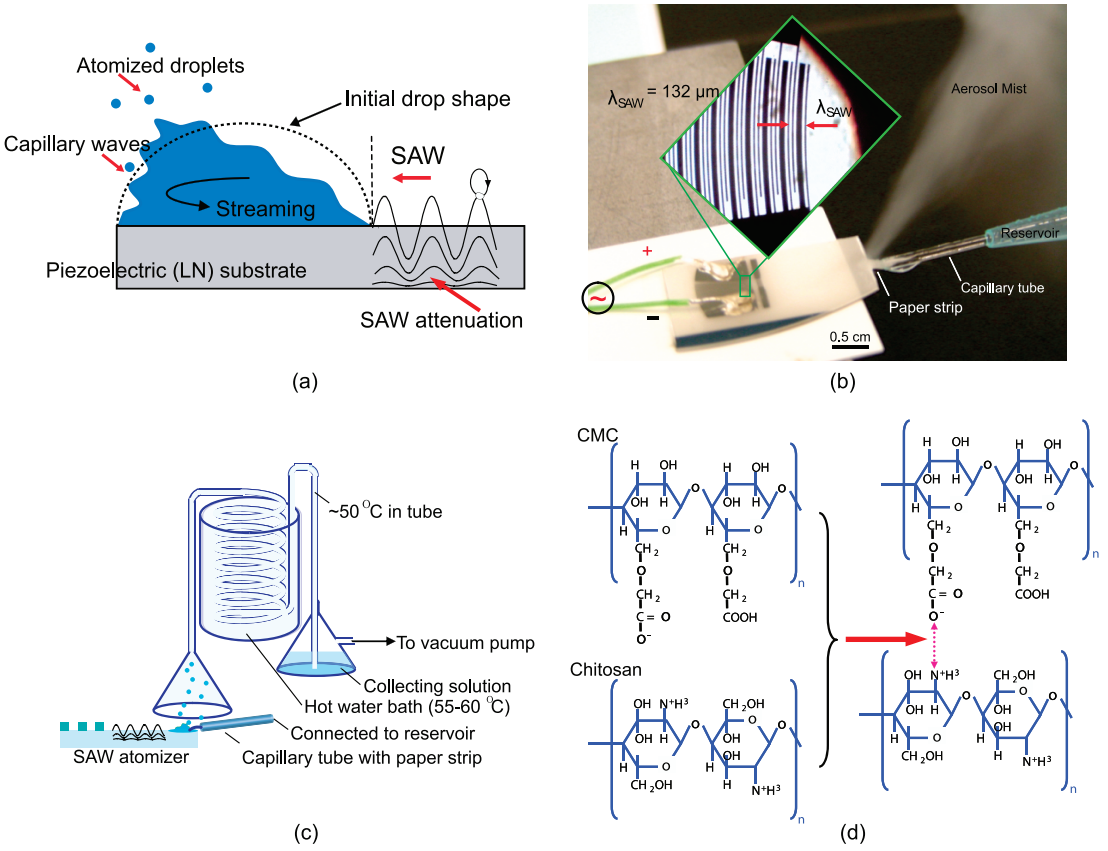

Figure 1. (a) Depiction of the atomization process: SAW leakage into a millimeter-dimension sessile drop placed on the piezoelectric substrate rapidly destabilizes and breaks up the interface to produce micrometer-sized aerosol droplets.[19] Note that the SAWs have amplitudes of around 1−10 nm and hence are not drawn to scale. (b) Image of the experimental setup showing the SAW device on which finger pairs of the single-phase unidirectional transducer (SPUDT) electrode are patterned (enlarged in the inset). The working fluid is delivered from a reservoir to the SAW substrate through the capillary wicking action of a small paper strip placed at the tip of a shortened capillary tube. (c) Schematic illustration of the experimental setup used to synthesize a nanocarrier comprising a single polymer. The polymer, dissolved in an appropriate solvent and held in a reservoir is fed *via* the capillary tube and paper wick to the SAW device to be atomized. The solvent in the aerosol droplets then evaporate in-flight within the conical funnel and spiral tube, aided through heating of the tube by immersing the entire assembly in a hot water bath. The solidified polymer nanocarriers that remain are then channeled into a collecting solution that consists of the complementary polymer that is to form the next layer, dissolved in an appropriate solvent. This suspension is then fed to the SAW device and reatomized using the same setup to obtain the next polymer layer. Further layers can simply be obtained by repeating the entire process for as many times as the number of layers desired. (d) Ionic complexation between chitosan and carboxymethyl cellulose (CMC).

compositional analysis of the nanocarriers using Fourier transform infrared spectroscopy. Together with microscopy and fluorescence imaging, these constitute a culmination of the main techniques used in recent studies,[29−32] among others; we refrain from carrying out characterization using a quartz crystal microbalance since this can only verify layer deposition of thin films on *planar substrates* rather than on *nanoparticles*. Encapsulation of pDNA, for example, within the polymer layer(s) may be accomplished by dispersing them within the initial polymer solution that is atomized to form the carrier's core.

Size distribution. Figure 2a shows particle size distributions obtained using dynamic light scattering (DLS) for the various nanocarriers. Their 100 nm order dimension, one order of magnitude smaller than that obtained using microfluidic LbL technology[12,13] and within the desirable range for targeted delivery, particularly for cancer therapy,[16,17] is confirmed by the atomic force microscopy (AFM) images shown in the inset of Figure 2a. This is representative of images obtained over many samples; the AFM-measured diameter is slightly smaller than the DLS-determined hydrodynamic diameter due to the swelling of polymeric particles in the presence of solvents common in DLS measurements.[33] The images also reveal that the nanocarriers assume a slightly oval shape, possibly due to the rigid and extended conformation of CMC. Quite counterintuitively, however, we observe the mean nanocarrier diameter in Figure 2a to *decrease* with the addition of a successive polyelectrolyte layer or the encapsulation of pDNA: 322.5 nm (standard deviation 64.3 nm) for sample A (Chi nanocarriers suspended in CMC solution), 198.2 nm (standard deviation 56.8 nm) for sample B (Chi/CMC bilayer nanocarriers), and 162.7 nm (standard deviation 89.4 nm) for sample

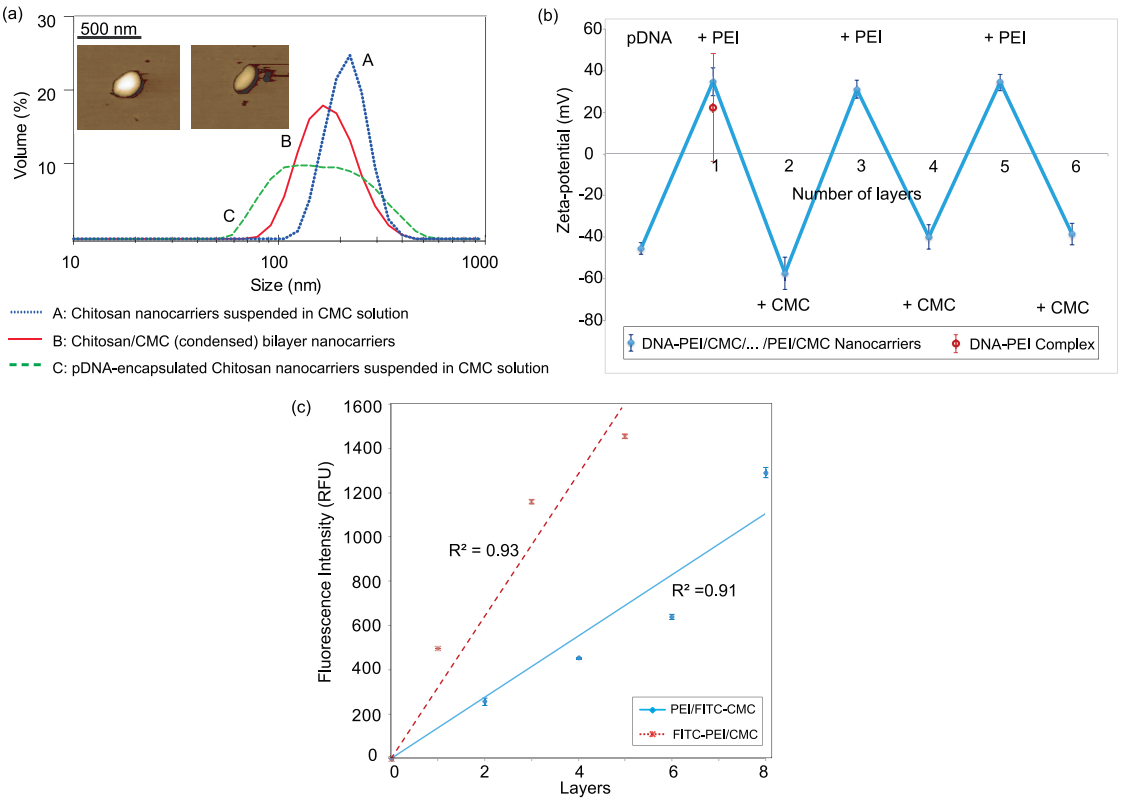

Figure 2. (a) Nanocarrier size distribution from dynamic light scattering experiments for Chi nanocarriers suspended in CMC solution (sample A), Chi/CMC bilayer nanocarriers (sample B) generated by atomizing sample A, and, pDNA-encapsulated Chi nanocarriers suspended in CMC solution (sample C). The inset shows representative AFM images of Chi/CMC bilayer nanocarriers. The diameter across the oval-shaped nanocarrier is typically between 150−300 nm, falling within the size distribution obtained by DLS. (b) Zeta-potential measurements of the outer layer of PEI/CMC nanocarriers encapsulated with pDNA, obtained after every successive layering step; also shown is the large variation in the zeta-potential measurements for the direct complexation of pDNA and PEI. We note that for each sample, the zeta-potential alternated between positive and negative, thus verifying that alternating complementary layers of PEI and CMC were successfully deposited in turn. (c) Intensity measurements (in relative fluorescence units, RFUs) of the fluorescence emitted by successive layers of the nanocarriers wherein one of the two complementary polyelectrolytes has been labeled with fluorescein isothiocyanate (FITC) (dashed line, nanocarriers comprising alternate layers of FITC labeled PEI and label-free CMC; solid line, nanocarriers comprising alternate layers of FITC labeled CMC and label-free PEI). The measurements were taken after each layering step and the lines indicate linear regression of the data using a least squares fit, showing the departure from linearity.

C (pDNA-encapsulated Chi nanocarriers suspended in CMC solution). The size decrease upon deposition of the CMC layer over the Chi core could be due to the strong electrostatic attraction of the adsorbed polyelectrolyte layer to the oppositely charged polyelectrolyte core, resulting in the condensation of both polymers. The observed size decrease when pDNA is encapsulated within Chi can be attributed to DNA condensation into compact structures as a result of polycation adsorption,[34] possibly due to ionic complexation.[35]

While fairly broad, the size distribution is typically acceptable in a number of applications; more importantly, the nanocarriers have not been filtered after synthesis, which also has the associated downside of potential loss of material. This is in contrast to the typical approach used for other processes where filtering is a key step in obtaining the desired results at the cost of yield efficiency. In any case, the nanocarrier size and size distribution as well as the thickness of the layers can be controlled through the atomizing fluid's physical properties (*e.g.*, viscosity and surface tension); these are known to strongly influence the destabilization wavelength, the aerosol size, and hence the nanocarrier dimension.[19] Surfactants to alter the surface tension or glycerine to modify the viscosity, for example, have been used to control nanoparticle size as well as its size distribution;[24,25] together with the judicious choice of the SAW operating frequency among the fundamental and harmonic resonances of the electrode and its various designs, it is thus possible to control the nanocarrier size and morphology. Nevertheless, a detailed study on the control of the nanocarrier size and distribution as well as its layer morphology is beyond the scope of this proof-of-concept study, constituting a topic for thorough investigation to be reported subsequently.

Spectroscopy. Figure 3 reveals the Fourier transform infrared (FT-IR) spectra for the pure CMC (curve A), pure Chi (curve B), Chi/CMC/Chi trilayer (curve C), and Chi/CMC bilayer (curve D) nanocarriers, respectively. Two

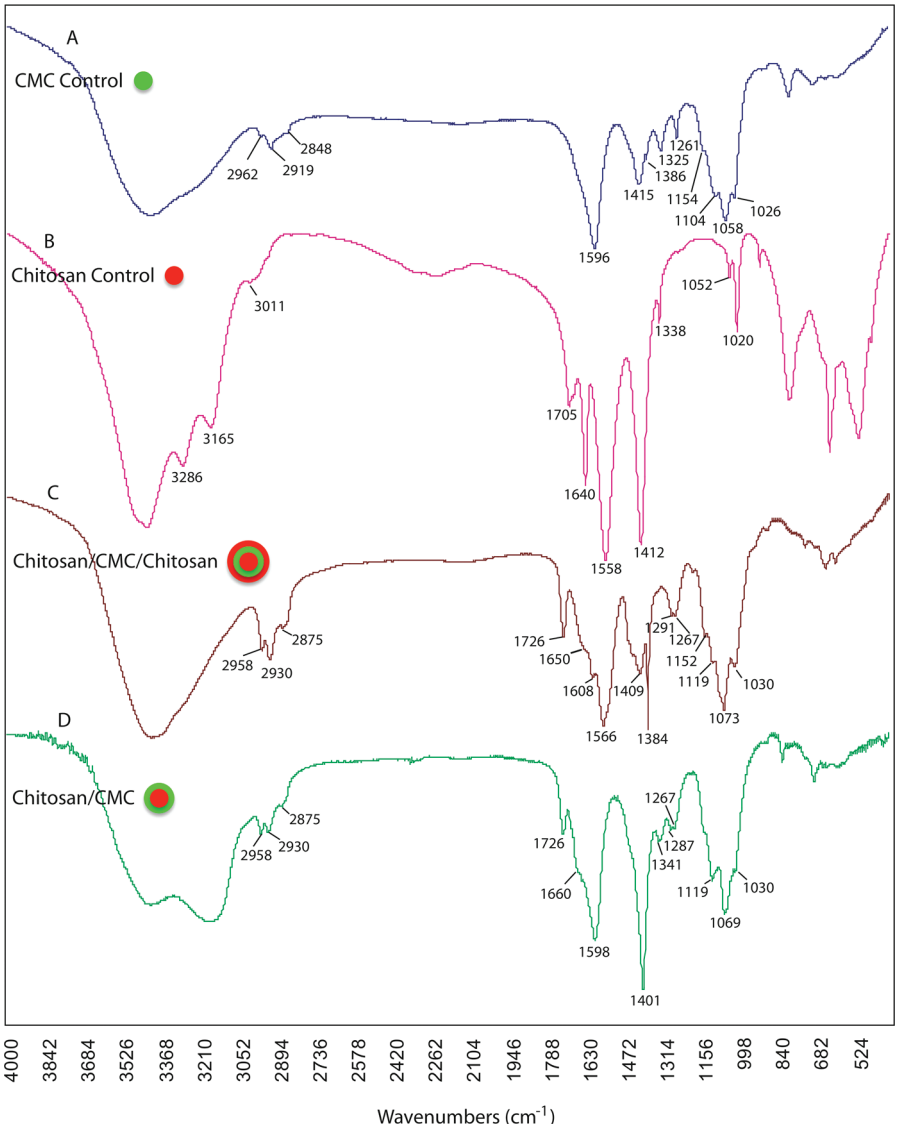

Figure 3. FT-IR spectra for the pure CMC (curve A), pure Chi (curve B), Chi/CMC/Chi trilayer (curve C), and Chi/CMC bilayer (curve D) nanocarriers, respectively. The different characteristic spectra of both trilayer and bilayer (curves C and D, respectively) nanocarriers from pure CMC and Chi (curves A and B, respectively) indicate that ionic complexation between the $-NH_2$ groups in Chi and $-COOH$ groups in CMC has taken place.

characteristic bands at 1596 and 1415 cm^{-1} can be seen for pure CMC (curve A), and can be attributed to the asymmetric and symmetric stretching of the carboxylate group, respectively. Characteristic bands at 1154, 1058, and 1026 cm^{-1}, on the other hand, correspond to the polysaccharide skeletons of the CMC molecule.[36] For the Chi spectrum (curve B), characteristic bands at 1640 and 1558 cm^{-1} are associated with the amide I and amide II peaks, respectively, whereas the bands at 1052 and 1020 cm^{-1} are characteristic of the polysaccharide skeleton of the Chi molecule.[37] Clearly, curves C and D show characteristic spectra different from that of pure CMC and Chi. The amide I band at 1640 cm^{-1} in the bilayer and trilayer nanocarriers has shifted to 1660 and 1650 cm^{-1}, respectively, reflecting the interactions between the $-COOH$ groups in the CMC molecule and the $-NH_2$ groups in the Chi molecule. The shift in the characteristic bands corresponding to the polysaccharide skeletons for the multilayer nanocarriers in curves C and D also suggest that ionic complexation between Chi and CMC has taken place.

Zeta-Potential. Additional verification of the existence of successive polyelectrolyte layering within the nanocarriers can be obtained through zeta-potential measurements as the layers are formed. As shown in Figure 2b, the sign of the zeta-potential reverses as each alternating layer of PEI and CMC is deposited over the initial pDNA, which has a strong negative charge. The alternate reversal in the zeta-potential observed here is consistent with that observed in conventional LbL synthesis,[38] and confirms the consecutive deposition of successive layers on the nanocarrier comprising polyelectrolytes of opposite charge. We also note a considerable reduction in the variation in the zeta-potential

of the pDNA–PEI complex formed during the SAW atomization–evaporation process compared to that due to direct complexation, indicating that the atomization and evaporation leads to enhanced polyelectrolyte binding.

Fluorescence Intensity. Further evidence of the presence of multiple polyelectrolyte layers can be obtained by fluorescently labeling either PEI or CMC (while leaving the other complementary polymer pair unlabeled). Figure 2c shows the fluorescence intensity of the nanocarriers as additional layers of PEI and CMC are alternately deposited. We observe the fluorescence intensity to gradually increase, albeit nonlinearly, with the increase in nanocarrier mass upon the addition of each labeled polymer layer which binds *via* electrostatic interaction to the underlying polymer. Similar nonlinear increases in the fluorescence intensity with additional polymer layering have been reported elsewhere,[39,40] and reflects a complexated (as opposed to a core–shell) structure of the nanocarriers synthesized in the present work owing to the interpenetration of the polyelectrolyte molecules which are embedded and intertwined across multiple layers in a manner similar to that proposed by Ladam *et al.*[41] Other factors are also known to contribute to nonlinear growth of the fluorescence signal. The increase in surface area of the nanocarrier with the deposition of each additional layer, for example, allows greater polyelectrolyte and fluorophore coverage, leading to the departure in the linearity of the signal intensity especially when the thickness of the deposited layers are non-negligible compared to the nanocarrier dimension.[39] This is a plausible explanation for the trend observed for the labeled CMC (solid line). On the other hand, the size of the polyelectrolyte can also influence its coverage and hence the fluorescence signal.[40] A larger number of short polyelectrolytes, for example, are required to saturate the nanocarrier surface compared to the case of longer polyelectrolytes, and may explain the faster initial rate of increase for PEI (25 kDa) compared to that for CMC (90 kDa). The increase in fluorescence intensity for labeled PEI (dotted line) is however observed to taper off as the number of layers increases, possibly due to self-quenching of the fluorophores.[42] The shorter PEI chains allow more efficient penetration into the voids that form due to heterogeneous deposition of prior layers,[41] resulting in more compacted structures with higher coverage densities. The close packing between the fluorophore molecules as a consequence is known to lead to lower fluorescence yields due to fluorophore self-quenching.[39,42]

***In Vitro* pDNA Release.** Figure 4 shows the *in vitro* release profile of encapsulated pDNA from both Chi/CMC bilayer (sample A) and Chi/CMC/Chi trilayer (sample B) nanocarriers. Unbound/excess pDNA adhering to the outer shell of the nanocarriers appears to provide an initial burst in the release profile over about

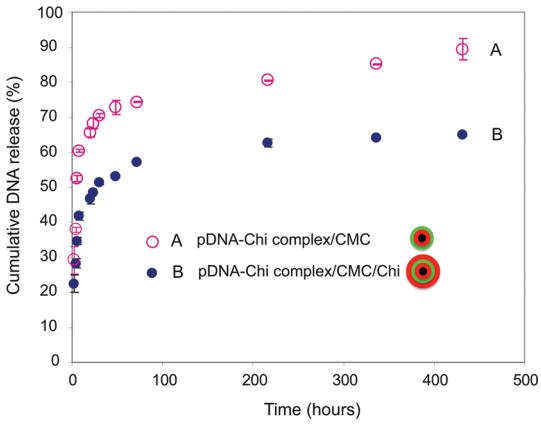

Figure 4. *In vitro* release profile for pDNA encapsulated in Chi/CMC bilayer (sample A) and Chi/CMC/Chi trilayer (sample B) nanocarriers over a period of 19 days.

5 h for both nanocarrier sets, followed by a slower continuous release of the pDNA encapsulated within the nanocarrier over several days. The additional Chi layer on sample B serves to dramatically slow the release of the encapsulated pDNA compared to sample A, releasing DNA over the course of 19 days. The quantized control of the release rate based on the number of polyelectrolyte layers deposited over the drug molecule is attractive from the standpoint of tailoring the drug carrier to the desired release dynamics. Slower release, for the delivery of plasmid encoding growth factors in regenerative medicine, for example, is achievable with more layers. Likewise, fast release–to initiate an immune response for DNA vaccination, for instance–is a matter of reducing the number of layers. The added control provided by the atomization process in manipulating the polymer materials, the N/P ratio between the DNA and polymer, and the polymer mass ratio, among other properties, should enable finely tailorable delivery solutions for a broad spectrum of drugs and serves as a means for studying the formation of specific nanocarriers to treat particular diseases in the future.

***In Vitro* Cell Transfection.** Given the susceptibility of pDNA to shear- or cavitation-induced lysis, gene transfection experiments were carried out to assess whether the nanocarriers and encapsulated plasmid DNA retain their viability and functionality throughout the synthesis. A yellow fluorescent protein (YFP) reporter gene-encoded plasmid was encapsulated in a PEI/CMC bilayer nanocarrier and transfected into mammalian COS-7 and human mesenchymal progenitor cells (MPCs); COS-7 cells represent a target for cellular engineering applications (*e.g.*, protein overexpression, *etc.*), whereas MPCs represent a potent target for stem cell therapy applications. Qualitative evidence of successful gene survival and transfection by pDNA encapsulated within the PEI/CMC nanocarriers is illustrated through the fluorescence expressed by the YFP (depicted in green) in the cytoplasm of both COS-7 cells and MPCs observed in

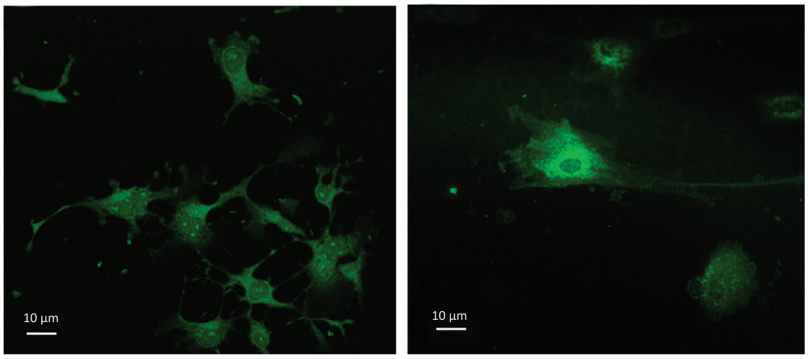

Figure 5. Confocal laser scanning microscopy images of (a) COS-7 cells and (b) MPCs transfected with pVR1020-YFP encapsulated within PEI/CMC bilayer nanocarriers. The cells exhibited granular fluorescent spots distributed throughout the cytoplasm 72 h post-transfection.

the confocal microscopy images taken 72 h post-transfection (Figure 5). The nanocarrier synthesis and plasmid encapsulation using the SAW does not appear to cause degradation of the pDNA—a result consistent with our previous studies reporting postatomization cell and molecular viability.[25,26] On the basis of the evidence from the size distributions reported above, the surrounding polyelectrolyte layers of the nanocarriers appear to condense the DNA into a much more compact structure, thereby shielding them from shear, heat, and possibly other means of degradation.

CONCLUSIONS

A new technique to synthesize multilayer polyelectrolyte nanocarriers using surface acoustic wave atomization is demonstrated. Evidence of the consecutive layering of oppositely charged polyelectrolytes and pDNA is shown through FT-IR spectroscopy and zeta-potential measurements, in addition to AFM and fluorescence imaging. In contrast to conventional benchtop procedures, the method offers a low cost, rapid, and simple synthesis route, in addition to circumventing the limitations associated with conventional and microfluidic layer-by-layer formation techniques, namely, the necessity of sacrificial colloidal templates in the former and the large *micro*carrier dimensions in the latter, as well as the difficulties of encapsulation typically encountered. Nanocarriers with up to eight alternating complementary polyelectrolyte layers were synthesized in this study, although additional layers can be deposited in principle simply by successively repeating the atomization—evaporation—resuspension layering process. The nanocarriers have dimensions of around 200 nm or less, which is attractive from the perspective of targeted drug delivery applications. Further, we demonstrate the possibility of encapsulating therapeutic molecules within the multilayered nanostructures using pDNA as a model drug. The additional polyelectrolyte layer is observed to slow down the release rate considerably, therefore offering the opportunity for tuning the release of the drug simply by altering the number of deposited layers. Finally, we verify *in vitro* gene transfection of pDNA-encapsulated nanocarriers into human mesenchymal progenitor and mammalian COS-7 cells. The gene expression in these cells not only indicates that the functionality of the pDNA is preserved during synthesis but also provides evidence of the transfection ability of the therapeutic agents encapsulated within the multilayer nanocarriers for a host of gene delivery applications.

METHODS

SAW Device. Together with standard UV photolithography and wet-etching, a single-phase unidirectional transducer (SPUDT) electrode was sputter-deposited (Hummer Triple Target Magnetron Sputter System, Anatech, Orange, MA, USA) onto a 127.68° *y*-cut *x*-propagating single crystal lithium niobate (LN) substrate (Roditi Ltd., London, UK), as shown in Figure 1b. The width and gap of the SPUDT finger patterns specify the SAW frequency—in this case, the SPUDT is patterned to produce a SAW with 30 MHz resonant frequency corresponding to a wavelength of 132 μm. To generate the SAW, an oscillating electrical signal at the resonant frequency is supplied to the SPUDT using a signal generator (SML01, Rhode & Schwarz, Munich, Germany) and amplifier (model 10W1000C, Amplifier Research, Souderton, PA, USA). To facilitate delivery of the working fluid to the SAW device for atomization, a short paper (Polyester-Cellulose, LymTech, Chicopee, USA) wick was placed at the tip of a shortened capillary tube connected to a reservoir (Figure 1b).

Nanocarrier Generation. The rest of the experimental setup is schematically illustrated in Figure 1c. The SAW device together with the capillary tube connected to the reservoir containing the polymer solution to be atomized is mounted securely under a conical funnel leading to a spiral tube assembly submerged in a water bath maintained at approximately 40—50 °C. The other end of the spiral tube is submerged in the oppositely charged complementary polymer solution placed within a glass flask. As a consequence of atomizing the initial polymer solution, the aerosols generated navigate through the heated spiral tube. During this process, the solvent in the aerosol droplets evaporate

and hence leave behind solidified polymer nanocarriers. These nanocarriers were then deposited in the collection solution containing a polymer of opposite charge—the polymer system that is to constitute the subsequent layer over the initial polymer core—dissolved in an appropriate solvent. Unbound polymer was removed by dialysis prior to further analysis. If an additional layer is desired, the nanocarrier suspension can be purified prior to their return to the SAW device for reatomization into an alternate polymer solution. This atomization–evaporation–resuspension process can be repeated as many times as the number of additional polymer layers desired.

Polymers. The model polymers employed comprised positively charged chitosan (Chi, MW ≈ 120 kDa) or linear polyethyleneimine (PEI, MW ≈ 25 kDa, Polysciences Inc., Warrington, PA, USA) and negatively charged carboxymethyl cellulose (CMC, MW ≈ 90 kDa). Chi and CMC are commonly used polymers for *in vivo* drug delivery given their biocompatibility and low cytotoxic nature.[43] Chi can efficiently condense pDNA and also increase the permeability of macromolecules across the gastrointestinal tract.[44] Linear PEI is well-known as an efficient carrier for pDNA delivery. In our experiments, PEI in water or Chi in sodium acetate buffer was atomized into CMC in water, and subsequently reatomized into another Chi or PEI solution. Unless stated otherwise, all reagents and solvents of biological grade were obtained from Sigma-Aldrich Pty. Ltd. (Castle Hill, NSW, Australia) and used without further purification.

Multilayer Nanocarrier Characterization. To demonstrate the bonding between successive polyelectrolyte layers and hence provide evidence of the existence of each layer, we examined the properties of the nanocarriers at every step of the LbL technique prior to reatomization. Several characterization techniques were employed as described as follows:

Size Distribution. Immediately after each atomization–evaporation–resuspension process, the hydrodynamic diameter of the nanocarriers was measured using dynamic light scattering (DLS; Zetasizer Nano S, Malvern Instruments Ltd., UK). Atomic force microscopy (AFM; NT-MDT Ntegra, Zelenograd, Russia) was also used to observe the individual nanocarrier morphologies. In addition, visual inspection of their dimensions also provide additional verification to that obtained using DLS.

Spectroscopy. The compositional analysis of multilayer nanocarriers was carried out using Fourier transform infrared spectroscopy (FT-IR spectrometer, Spectrum 100 series, PerkinElmer, Waltham, MA, USA). Prior to the analysis, the synthesized nanocarriers were recovered through dialysis followed by lyophilization.

Zeta-Potential. We expect the zeta-potential of the nanocarrier to reverse with the successive deposition of each additional layer of alternately charged polyelectrolyte. The zeta-potential of the nanocarriers was measured after each layering step using an electrophoretic light scattering spectrophotometer (Zetasizer Nano S, Malvern Instruments, Malvern, UK).

Fluorescence Intensity. The sequential bonding of each successive polyelectrolyte layer onto the surface of the nanocarrier was detected by selectively labeling the polymers. Fluorescein isothiocyanate (FITC) labeled CMC was prepared by activating CMC using 0.318 mmol of N-hydroxysuccinimide and 0.318 mmol of N-(3-dimethylaminopropyl)-N-ethylcarbodiimide hydrochloride in 100 mL of deionized (DI) water followed by dropwise addition of 0.318 mmol fluoresceinamine dissolved in methanol. The reaction was performed at pH 4.7 and at room temperature for 24 h in the dark. FITC labeled PEI was prepared by adding 90.4 mg of fluorescein-5-isothiocyanate (Invitrogen Corp., Carlsbad, CA, USA) dissolved in 2 mL of dimethylsulfoxide dropwise to 1 g of PEI dissolved in water. The reaction was performed at room temperature for 24 h in the dark. The labeled polymers were purified by dialysis against running water (MWCO 3500 dialysis tubing, Spectrum Laboratories, Rancho Dominguez, CA, USA) for 3 days in the dark and freeze dried. Multilayer nanocarriers composed of FITC labeled PEI and label-free CMC, or, FITC labeled CMC and label-free PEI were prepared using the atomization procedures described above. Fluorescence measurements were carried out on a multimode spectrophotometer (SpectraMax M2, Molecular Devices, Sunnyvale, CA, USA) under excitation and emission wavelengths of 490 and 525 nm, respectively.

pDNA Encapsulation and *in Vitro* Release. Plasmid DNA pEGFP-N1 (4733bp, 1.8×10^6 g/mol, Clontech Laboratories Inc., Mountain View, CA, USA) was employed as a therapeutic gene model. The plasmid was first added to the Chi solution to form a pDNA–Chi complex and subsequently atomized into the CMC solution, which was then reatomized into the Chi solution to form the Chi/CMC bilayer nanocarrier within which the pDNA is trapped. To form the encapsulated Chi/CMC/Chi trilayer nanocarrier, an additional layering step was performed. The pDNA release study was carried out under near-physiological conditions. Briefly, the pDNA-encapsulated nanocarriers were dispersed in acetate buffer inside a dialysis bag, which was then immersed in agitated acetate buffer at 37 °C to simulate the pH of the endosomal (pH ~6) and lysosomal (pH ~5) microenvironments. Samples were collected at different time intervals for pDNA quantification using the Quant-iT PicoGreen dsDNA reagent (Invitrogen Corp., Carlsbad, CA, USA) assay according to the manufacturer's guidelines. The fluorescent intensity was measured using the multi-mode spectrophotometer under excitation and emission wavelengths of 490 nm and 525 nm, respectively. The cumulative fraction release was normalized with respect to the total amount of pDNA encapsulated in the nanocarriers.

***In Vitro* Cell Transfection.** African green monkey kidney COS-7 cells acquired from the American Type Culture Collection (ATCC, Rockville, MD, USA) were cultured in DMEM following the protocol supplied. Human mesenchymal progenitor cells (MPC) obtained from the Monash Institute of Medical Research (Clayton, VIC, Australia) were separately maintained in complete DMEM medium, supplemented with 10% fetal bovine serum (FBS), 100 μM L-ascorbate-2-phosphate magnesium, 2 mM L-glutamine and 50 units/mL penicillin–streptomycin at 37 °C in a humidified 5% carbon dioxide incubator.

Cells were seeded at 80% confluence on a four-well Lab-Tek chambered coverglass (Nunc GmbH & Co. KG, Langenselbold, Germany) and grown overnight. Bilayer PEI/CMC nanocarriers encapsulating DNA vaccine-type plasmid pVR1020 encoding yellow fluorescent protein reporter (pVR1020-YFP) were prepared using the same procedures described above under aseptic conditions. The spent media was removed and replaced with DMEM containing 2% FBS. Nanocarriers containing 10 μg of plasmid were added to the cells and allowed to incubate for 4 h, following which the medium was removed and replaced with growth medium. Each control well received 3.75 mg of PEI reagent complexed with 10 μg DNA (N/P ratio = 5). After 72 h, cells were monitored for gene expression using confocal laser scanning microscopy (A1Rsi Multiphoton System, Nikon Pty. Ltd., Lidcombe, NSW, Australia) under excitation and emission wavelengths of 514 and 527 nm, respectively. The original grayscale images from the fluorescence channel were mapped to an arbitrary green color to represent the fluorescence of the YFP.

Acknowledgment. Funding for this work was provided through Australian Research Council Discovery (ARC) Project Grant DP2433214 and National Health and Medical Research Council (NHMRC) Development Grant 546238. L.Y.Y. is also grateful to the Australian Research Council for an Australian Research Fellowship under ARC Discovery Project Grant DP2433179. The authors acknowledge the help of Fatin Al-Deen (Chemical Engineering, Monash University) who provided assistance in obtaining preliminary fluorescence microscopy images and Adam Mechler (School of Molecular Sciences, La Trobe University) for his assistance with acquiring the AFM images. We also thank Graham Jenkin (Monash Institute of Medical Research) for kindly supplying us with the stem cells and Justin Cooper-White and Dmitry Ovchinnikov (University of Queensland) for helpful discussions regarding the work and early attempts with the *in vitro* transfection.

REFERENCES AND NOTES

1. LaVan, D. A.; McGuire, T.; Langer, R. Small-scale systems for *in vivo* drug delivery. *Nat. Biotechnol.* **2003**, *21*, 1184–1191.
2. Johnston, A. P.; Cortez, C.; Angelatos, A. S.; Caruso, F. Layer-by-layer engineered capsules and their applications. *Curr. Opin. Colloid Interface Sci.* **2006**, *11*, 203–209.

3. Shchukin, D. G.; Sukhorukov, G. B. Nanoparticle synthesis in engineered organic nanoscale reactors. *Adv. Mater.* **2004**, *16*, 671–682.
4. Decher, G. Fuzzy nanoassemblies: Toward layered polymeric multicomposites. *Science* **1997**, *277*, 1232–1237.
5. Caruso, F.; Caruso, R. A.; Möhwald, H. Nanoengineering of inorganic and hybrid hollow spheres by colloidal templating. *Science* **1998**, *282*, 1111–1113.
6. Sukhorukov, G. B.; Antipov, A. A.; Voigt, A.; Donath, E.; Möhwald, H. pH-controlled macromolecule encapsulation in and release from polyelectrolyte multilayer nanocapsules. *Macromol. Rapid Commun.* **2001**, *22*, 44–46.
7. Peyratout, C.; Dähne, L. Tailor-made polyelectrolyte microcapsules: From multilayers to smart containers. *Angew. Chem., Int. Ed.* **2004**, *43*, 3762–3783.
8. Khopade, A.; Caruso, F. Stepwise self-assembled poly(amidoamine) dendrimer and poly(styrenesulfonate) microcapsules as sustained delivery vehicles. *Biomacromolecules* **2002**, *3*, 1154–1162.
9. Caruso, F.; Trau, D.; Möhwald, H. Renneberg, Enzyme encapsulation in layer-by-layer engineered polymer multilayer capsules. *Langmuir* **2000**, *16*, 1485–1488.
10. Zhu, Y.; Shi, J.; Shen, W.; Dong, X.; Feng, J.; Ruan, M.; Li, Y. Stimuli-responsive controlled drug release from a hollow mesoporous silica sphere/polyelectrolyte multilayer core−shell structure. *Angew. Chem., Int. Ed.* **2005**, *44*, 5083–5087.
11. Shchukin, D. G.; Kommireddy, D. S.; Zhao, Y.; Cui, T.; Sukhorukov, G. B.; Lvov, Y. M. Polyelectrolyte micropatterning using a laminar-flowmicrofluidic device. *Adv. Mater.* **2004**, *16*, 389–393.
12. Priest, C.; Quinn, A.; Postma, A.; Zelikin, A. N.; Ralston, J.; Caruso, F. Microfluidic polymer multilayer adsorption on liquid crystal droplets for microcapsule synthesis. *Lab Chip* **2008**, *8*, 2182–2187.
13. Wong E. H. m. The development of a continuous encapsulation method in a microfluidic device. Ph.D. Thesis, The University of Queensland, Australia, 2009.
14. Kreuter, J. Nanoparticulate systems for brain delivery of drugs. *Adv. Drug Delivery Rev.* **2001**, *47*, 65–81.
15. Wissing, S. A.; Kayser, O.; Müller, R. H. Solid lipid nanoparticles for parenteral drug delivery. *Adv. Drug Delivery Rev.* **2004**, *56*, 1257–1272.
16. Yuan, F.; Dellian, M.; Fukumura, D.; Leunig, M.; Berk, D. A.; Torchilin, V. P.; Jain, R. K. Vascular permeability in a human tumor xenograft: Molecular size dependence and cutoff size. *Cancer Res.* **1995**, *55*, 3752–3756.
17. Gu, F. X.; Karnik, R.; Wang, A. Z.; Alexis, F.; Levy-Nissenbaum, E.; Hong, S.; Langer, R. S.; Farokhzad, O. C. Targeted nanoparticles for cancer therapy. *Nano Today* **2007**, *2- 3*, 14–21.
18. Friend, J.; Yeo, L. Y. Microscale acoustofluidics: microfluidics driven *via* acoustics and ultrasonics. *Rev. Mod. Phys.* **2011**, *83*, 647–704.
19. Qi, A.; Yeo, L. Y.; Friend, J. R. Interfacial destabilization and atomization driven by surface acoustic waves. *Phys. Fluids* **2008**, *20*, 074103.
20. Qi, A.; Yeo, L. Y.; Friend, J.; Ho, J. The extraction of liquid, protein molecules and yeast cells from paper through surface acoustic wave atomization. *Lab Chip* **2010**, *10*, 470–476.
21. Heron, S. R.; Wilson, R.; Shaffer, S. A.; Goodlett, D. R.; Cooper, J. M. Surface acoustic wave nebulization of peptides as a microfluidic interface for mass spectrometry. *Anal. Chem.* **2010**, *82*, 3985–3989.
22. Ho, J.; Tan, M. K.; Go, D.; Yeo, L. Y.; Friend, J.; Chang, H.-C. A paper-based microfluidic surface acoustic wave sample delivery and ionization source for rapid and sensitive ambient mass spectrometry. *Anal. Chem.* **2011**, *83*, 3260–3266.
23. Qi, A.; Friend, J. R.; Yeo, L. Y. Miniature inhalation therapy platform using surface acoustic wave microfluidic atomization. *Lab Chip* **2009**, *9*, 2184–2193.
24. Friend, J. R.; Yeo, L. Y.; Arifin, D. R.; Mechler, A. Evaporative self-assembly assisted synthesis of polymeric nanoparticles by surface acoustic wave atomization. *Nanotechnology* **2008**, *19*, 145301.
25. Alvarez, M.; Friend, J.; Yeo, L. Y. Rapid generation of protein aerosols and nanoparticles *via* surface acoustic wave atomization. *Nanotechnology* **2008**, *19*, 455103.
26. Alvarez, M.; Yeo, L. Y.; Friend, J. R.; Jamriska, M. Rapid production of protein-loaded biodegradable microparticles using surface acoustic waves. *Biomicrofluidics* **2009**, *3*, 014102.
27. Li, H.; Friend, J.; Yeo, L.; Dasvarma, A.; Traianedes, K. Effect of surface acoustic waves on the viability, proliferation and differentiation of primary osteoblast-like cells. *Biomicrofluidics* **2009**, *3*, 034102.
28. Oxtoby, D. W. Vibrational relaxation in liquids. *Annu. Rev. Phys. Chem.* **1981**, *32*, 77–101.
29. Leung, M. K. M.; Such, G. K.; Johnston, A. P. R.; Biswas, D. P.; Zhu, Z.; Yan, Y.; Lutz, J.-F.; Caruso, F. Assembly and degradation of low-fouling click-functionalized poly(ethylene glycol)-based multilayer films and capsules. *Small* **2011**, *7*, 1075–1085.
30. Chong, S.-F.; Lee, J. H.; Zelikin, A. N.; Caruso, F. Tuning the permeability of polymer hydrogel capsules: An investigation of cross-linking density, membrane thickness, and cross-linkers. *Langmuir* **2011**, *27*, 1724–1730.
31. Cortez, C.; Quinn, J. F.; Hao, X.; Gudipati, C. S.; Stenzel, M. H.; Davis, T. P.; Caruso, F. Multilayer buildup and biofouling characteristics of PSS-b-PEG containing films. *Langmuir* **2011**, *26*, 9720–9727.
32. Shutava, T. G.; Balkundi, S. S.; Vangala, P.; Steffan, J. J.; Bigelow, R. L.; Cardelli, J. A.; OÕNeal, P.; Lvov, Y. M. Layer-by-layer-coated gelatin nanoparticles as a vehicle for delivery of natural polyphenols. *ACS Nano* **2009**, *3*, 1877–1885.
33. Minatti, E.; Viville, P.; Borsali, R.; Schappacher, M.; Deffieux, A.; Lazzaroni, R. Micellar morphological changes promoted by cyclization of PS-*b*-PI copolymer: DLS and AFM experiments. *Macromolecules* **2003**, *36*, 4125–4133.
34. Bloomfield, V. A. DNA condensation. *Curr. Opin. Struct. Biol.* **1996**, *6*, 334–341.
35. Danielsen, S.; Varum, K. M.; Stokke., B. T. Structural analysis of chitosan mediated DNA condensation by AFM: Influence of chitosan molecular parameters. *Biomacromolecules* **2004**, *5*, 928–936.
36. Biswal, D. R.; Singh, R. P. Characterisation of carboxymethyl cellulose and polyacrylamide graft copolymer. *Carbohyd. Polym.* **2004**, *57*, 379–387.
37. Rosca, C.; Popa, M. I.; Lisa, G.; Chitanu, G. C. Interaction of chitosan with natural or synthetic anionic polyelectrolytes. 1. The chitosan−carboxymethylcellulose complex. *Carbohyd. Polym.* **2005**, *62*, 35–41.
38. Katagiri, K.; Caruso, F. Monodisperse polyelectrolyte-supported asymmetric lipid-bilayer vesicles. *Adv. Mater.* **2005**, *17*, 738–743.
39. Johnston, A. P. R.; Zelikin, A. N.; Lee, L.; Caruso, F. Approaches to quantifying and visualizing polyelectrolyte multilayer film formation on particles. *Anal. Chem.* **2006**, *78*, 5913–5919.
40. Lee, L.; Johnston, A. P. R.; Caruso, F. Manipulating the salt and thermal stability of DNA multilayer films *via* oligonucleotide length. *Biomacromoleucles* **2008**, *9*, 3070–3078.
41. Ladam, G.; Schaad, P.; Voegel, J. C.; Schaaf, P.; Decher, G.; Cuisinier, F. *In situ* determination of the structural properties of initially deposited polyelectrolyte multilayers. *Langmuir* **2000**, *16*, 1249–1255.
42. Imhof, A.; Megens, M.; Engelberts, J. J.; de Lang, D. T. N.; Sprik, R.; Vos, W. L. Spectroscopy of fluorescein (FITC) dyed colloidal silica spheres. *J. Phys. Chem. B* **1999**, *103*, 1408–1415.
43. Boonsongrit, Y.; Mitrevej, A.; Mueller, B. W. Chitosan drug binding by ionic interaction. *Eur. J. Pharm. Biopharm.* **2006**, *62*, 267–274.
44. Bhavsar, M. D.; Amiji, M. M. Polymeric nano- and microparticle technologies for oral gene delivery. *Expert Opin. Drug Delivery* **2007**, *4*, 197–213.